LAWRENCE
LIVERMORE
NATIONAL
LABORATORY

UCRL-CONF-223329

Hydrodynamic Simulations and Soft X-ray Laser Interferometric Studies of Energy Transport in Tightly Focused Laser-Heated Aluminum Plasmas

J. Dunn, S.J. Moon, R.F. Smith, R. Keenan, J. Nilsen, J.R. Hunter, J. Filevich, J.J. Rocca, M.C. Marconi, V.N. Shlyaptsev

August 2, 2006

10th International Conference on X-ray Lasers
Berlin, Germany
August 21, 2006 through August 25, 2006

Hydrodynamic Simulations and Soft X-ray Laser Interferometric Studies of Energy Transport in Tightly Focused Laser-Heated Aluminum Plasmas

J. Dunn, S.J. Moon, R.F. Smith, R. Keenan, J. Nilsen, J.R. Hunter

Lawrence Livermore National Laboratory, Livermore, CA 94551

J. Filevich, J.J. Rocca, M.C. Marconi

NSF ERC for Extreme Ultraviolet Science and Technology and Dept. of Electrical and Computer Engineering, Colorado State University, Fort Collins, CO 80523

V.N. Shlyaptsev

University of California Davis-Livermore, Livermore, CA 94551

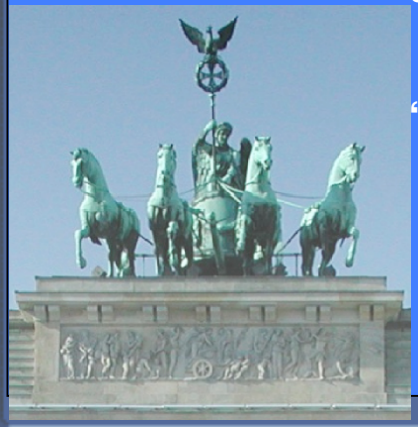

Presented at the:
"10th International Conference on X-ray Lasers"
Berlin, Germany 21 - 25 August, 2006

Work performed under the auspices of the US Department of Energy by the University of California Lawrence Livermore National Laboratory under Contract No. W-7405-Eng-48, through the Institute for Laser Science and Applications and in part by US Department of Energy grant No. #DE-FG52-06NA26152.

UCRL-CONF-223329

Overview

- Motivation
- Benefits of short wavelength ps probes for measuring plasmas
- X-ray laser interferometry setup and laser, target geometry
- Results
- Comparison with 2D LASNEX simulations
- Interpretation of energy transport mechanisms in small focal spot Al laser-produced plasmas leading to main plasma phenomena
- Summary

Motivation: High energy density plasma studies conducted uniquely with ultra-bright ps soft x-ray laser interferometry

Picosecond X-ray Laser Interferometry can:

- Measure 2-D $n_e(x, y, t)$
  - plasma evolution at different times
  - with picosecond time resolution
  - with ~1 μm spatial resolution
  - close to target surface
- Perform radiography and shadowgraphy
  - measure opacity, mixing
- Determine physical processes:
  - Ablation
  - Energy deposition and (non-)local heating
  - Production of converging plasmas
  - Formation of plasma jets
  - Shock unloading of surfaces

COMET Parameters for X-ray Laser

Parameters	COMET XRL
Pump (J):	5 J
XRL (J):	10 - 25 μJ
Photons/shot:	2×10^{12}
Rate (Hz):	0.004
λ (nm):	12 - 47
$\Delta\lambda / \lambda$:	$<10^{-4}$
Source (μm^2):	25 ×100
Div. ($mrad^2$):	2.5 ×10
Pulse (ps):	2 - 5
Peak B*:	1.6×10^{25}
Average B*:	1.3×10^{11}

* [Ph. mm^{-2} $mrad^{-2}$ s^{-1} (0.1% BW) $^{-1}$]

Greater understanding of energy transport mechanisms in LPP in order to check physics in hydrodynamic codes

Benefits of X-ray Laser Interferometry I: Earlier NOVA with 15.5 nm probe demonstrated reduced refraction and absorption

X-ray probes are deflected substantially less in plasma density gradients: probe higher density plasmas

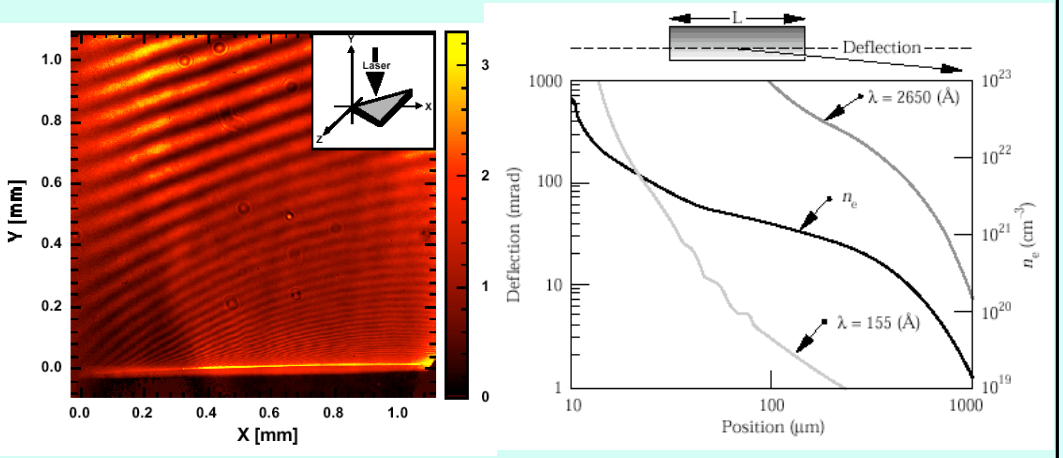

Da Silva *et al*, PRL 74, 3991 (1995).

For linear density gradient:

$$n_e = n_o\left[1-(y/y_o)\right]$$

Deflection angle scales as:

$$\theta \propto \lambda^2 L / y_o$$

Larger parameter space accessible to 15.5 nm x-ray laser

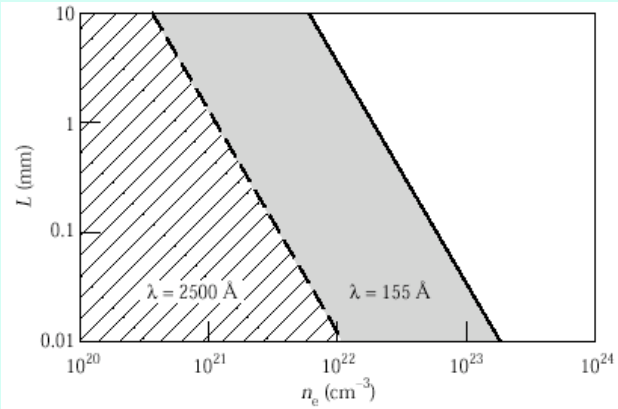

- **Only bremsstrahlung absorption considered**

$$\alpha = 2.42\times10^{-37}\frac{\langle Z^2\rangle n_e n_i}{\sqrt{T_e}(h\nu)^3}\left[1-\exp(-h\nu/kT_e)\right]$$

- **Abs. scales as $h\nu^{-2}$ if $h\nu \ll kT_e$**

Currently we have better time resolution, faster shot rate giving improved measurements to test simulation database

Benefits of X-ray Laser Interferometry II: RADEX shows reduced refraction with 14.7 nm allows probing close to target surface

Refraction of 4ω vs 14.7 nm of 1 mm Al plasma with shown density profile

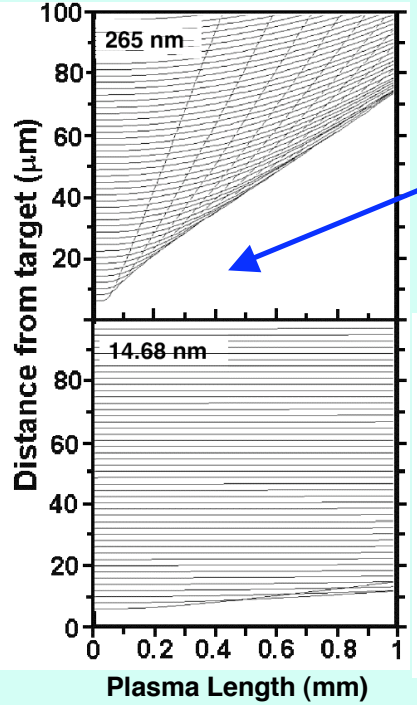

4ω cannot probe this region - limited to <50 μm long plasma

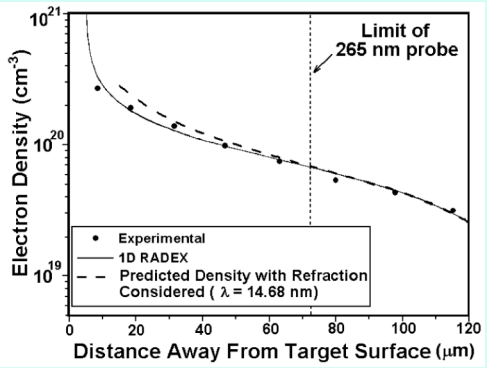

Al plasma, XRL at Δt = 700 ps

R. Smith *et al.*, JOSA B 20, 254 (2003).

Technical Advantages of X-ray Laser Interferometry

- 2 - 5 ps pulse duration measured
  - T_e ~ 100eV, v_s~ 5 x 10^6 cm/s
  - Δx~0.25μm, minimal plasma motion
- Short wavelength 14. 7 nm
  - Sub-micron spatial imaging
  - Reduced plasma absorption
  e.g. free-free abs.(~ λ^3 [1 - exp(-hc/λkT)])
  - Reduced plasma refraction (θ ~λ^2)
  - 4w probe requires *a priori* knowledge of plasma density to remove refraction
- Multilayer optics, gratings available for instrumentation
- Can be scaled to shorter wavelengths and Petawatt pumping for NIF experiments including hohlraums

X-ray laser interferometry combined with ps duration allows study of various LPP energy transport mechanisms at target surface

LLNL COMET facility generates synchronized x-ray laser probe for interferometry and plasma forming beam

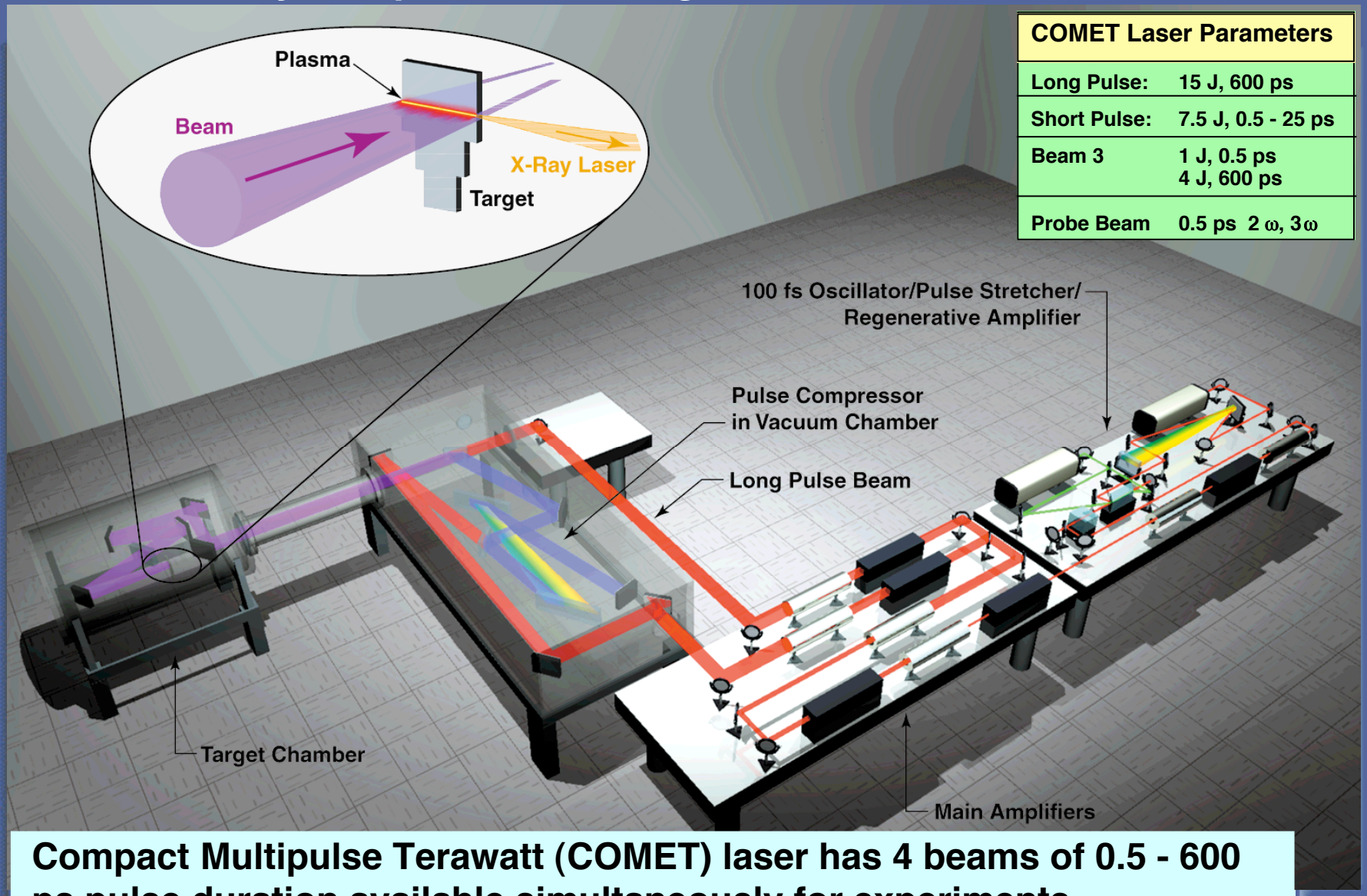

COMET Laser Parameters	
Long Pulse:	15 J, 600 ps
Short Pulse:	7.5 J, 0.5 - 25 ps
Beam 3	1 J, 0.5 ps 4 J, 600 ps
Probe Beam	0.5 ps 2 ω, 3 ω

Compact Multipulse Terawatt (COMET) laser has 4 beams of 0.5 - 600 ps pulse duration available simultaneously for experiments

Experimental setup: Laser energy, pulse shape and focal spot measured for irradiation of Al target plasma conditions

Measured Laser Focus and Pulse Shape

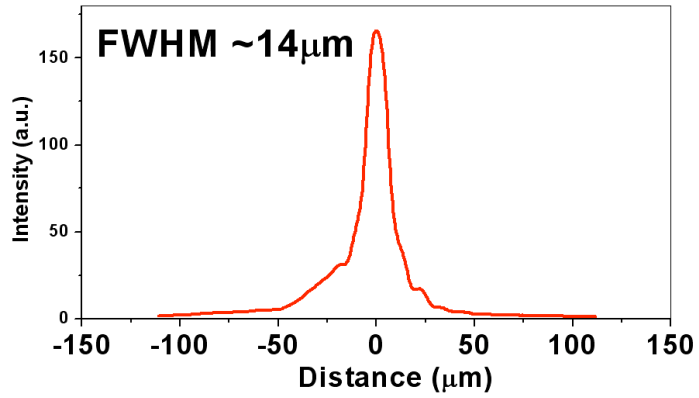

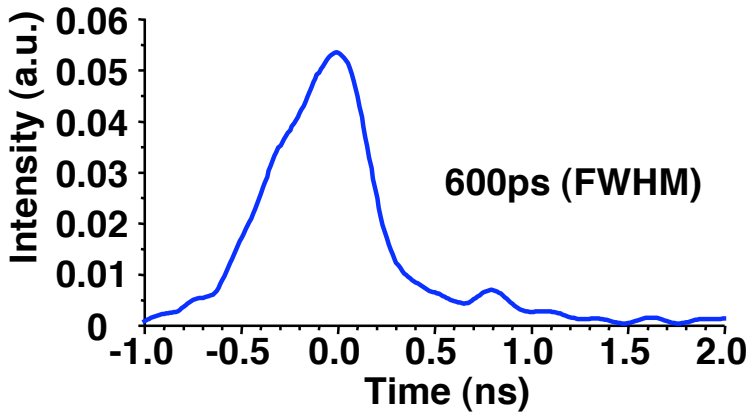

Experimental Setup

Al target heated:
- 3.1 J 1054 nm wavelength
- 600 ps (FWHM) pulse
- 14 μm x 0.32 cm wide line focus
- 1.2 x 10^{13} W cm^{-2}

X-ray laser probes longitudinally along plasma column

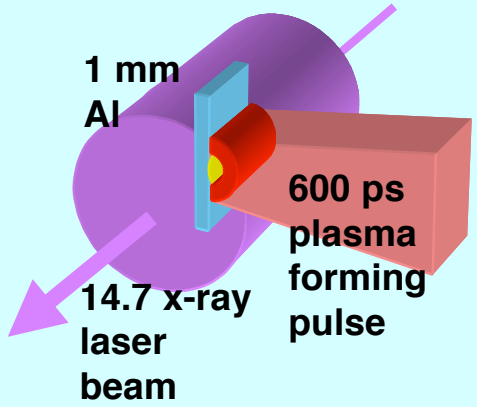

S. J. Moon *et al.*, in preparation for Physical Review E (2006).

X-ray Laser Interferometry Setup at 14. 7 nm: Skewed Mach-Zender geometry

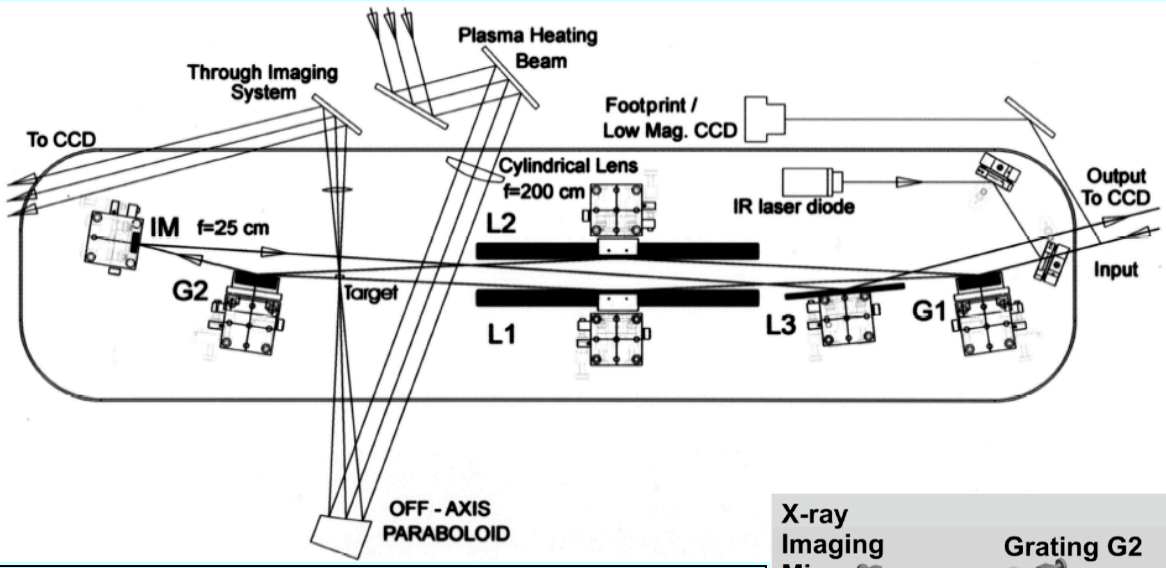

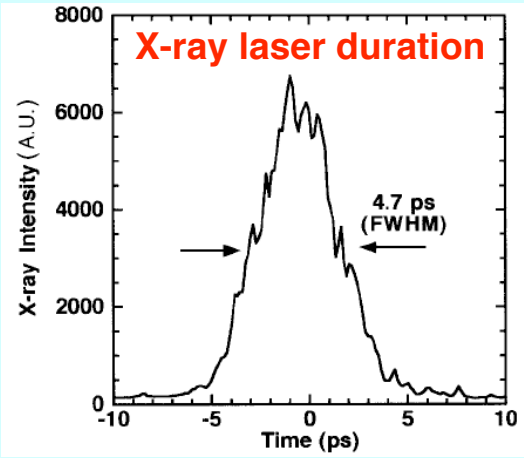

Notes:

Interferometer uses 0th and 1st orders

G1, G2 beam splitters: 900 l/mm

X-ray Imaging optic: Mo:Si coated *f* = 25 cm spherical mirror

Magnification: 22 x

Back-thinned CCD detector: 0.5 *μ*m spatial resolution

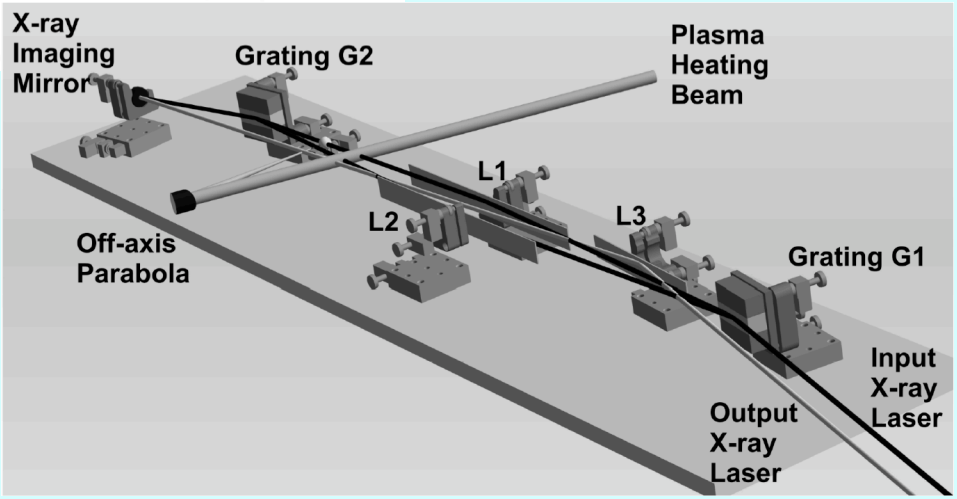

J. Filevich *et al.*, Appl Opt. 43, 3938 (2004).

At higher intensities, formation of density dip on-axis is observed very close to target surface and higher n_e

Al targets (1mm) heated by 3 J, 12 μm wide, 600 ps pulse at >10^{13} W cm^{-2}

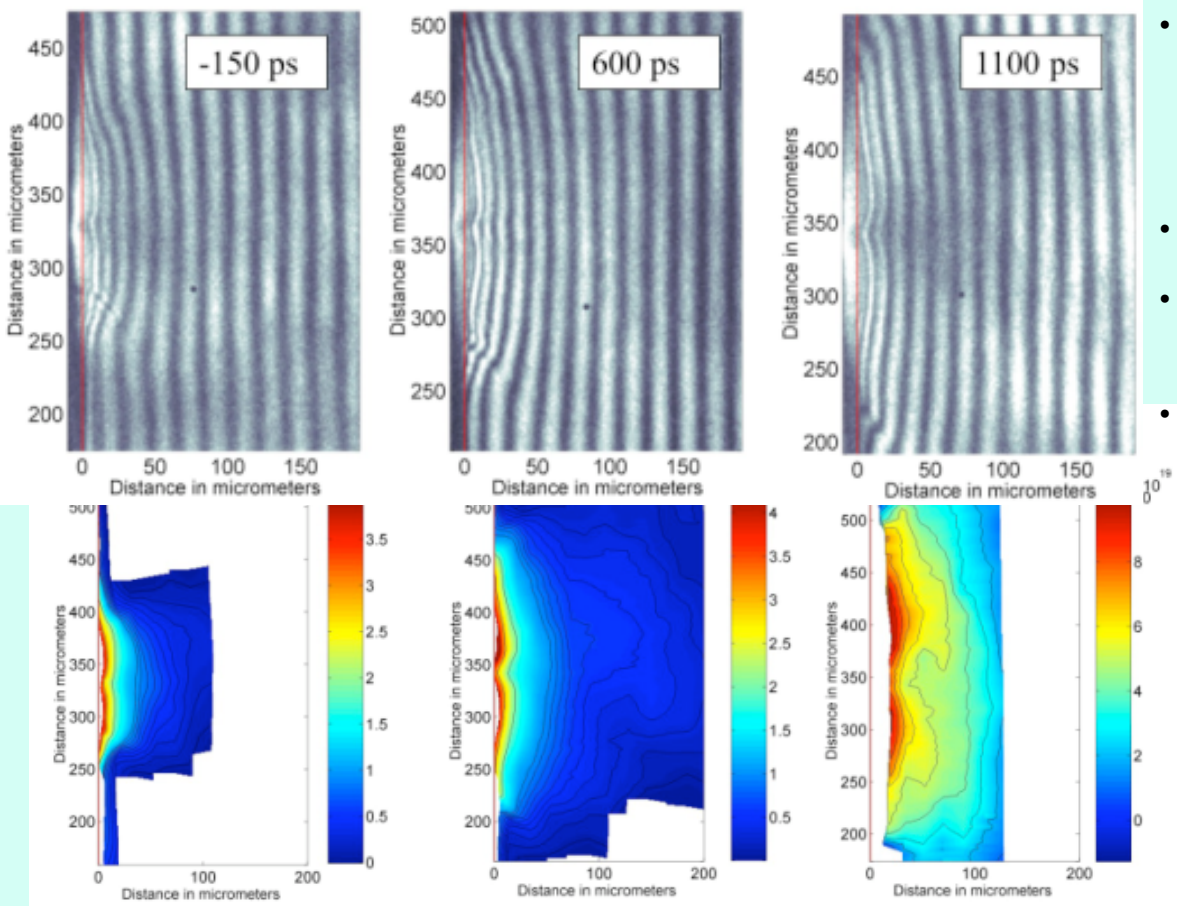

- Previously, flat targets irradiated at below 10^{12} W cm^{-2} have low n_e due to strong 2D effects
- 1 fringe = 1.5 x 10^{20} cm^{-3}
- Observe n_e > 4x10^{20} cm^{-3} at +0.6 ns for flat target
- Radiative heating and thermal conduction produces dense plasma in side lobes

* Long 12 ns heating expt.

J. Filevich, J. J. Rocca *et al*, "Two dimensional effects in laser-created plasmas measured with soft-x-ray laser interferometry", Phys. Rev. E 67, 056409 (2003).

On axis dip, formation of side lobes also observed previously*

Experimental results and comparison with 2D LASNEX simulations: Observe on-axis density dip, energy deposition outside of focus

Interferogram **Expt.** **2D Simulation** **2D LASNEX Details**

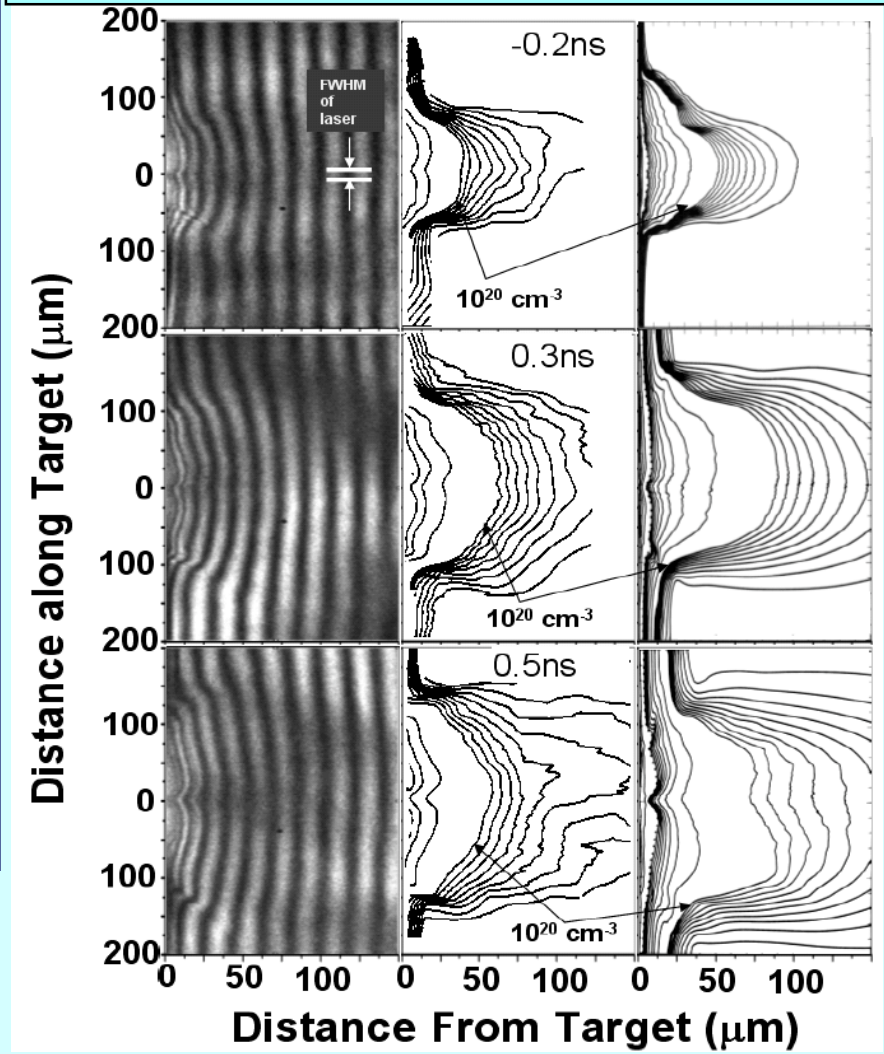

- Uses experimental spatial and temporal profile
- Inverse bremsstrahlung absorption
- Flux-limited multi-group diffusion, f=0.1 treated self-consistently
- Arbitrary Lagrangian Eulerian (ALE)
- 1 μm bins laterally, finer steps inside target
- Lee-More conductivity
- Livermore Equation of State (LEOS) (Ref. D. Young)
- 3D Laser ray-tracing package

1D or 1.5D hydrodynamics modeling would not adequately describe observed experimental features

Experimental results and comparison with 2D LASNEX simulations: Good quantitative agreement at various times

On-axis density profile comparison at -0.2, 0.3 and 0.5 ns

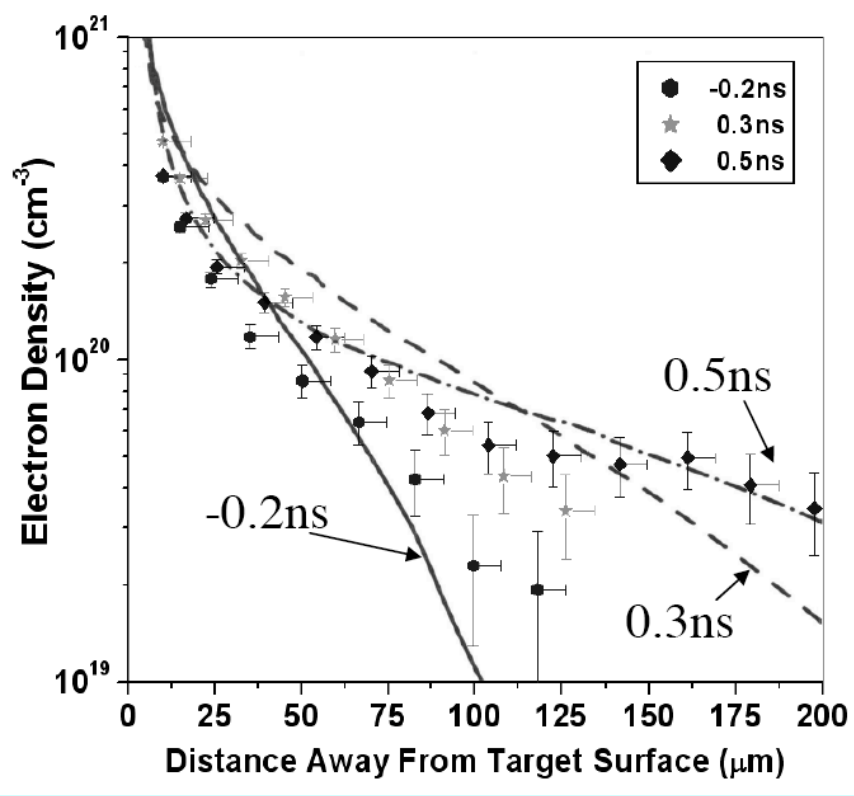

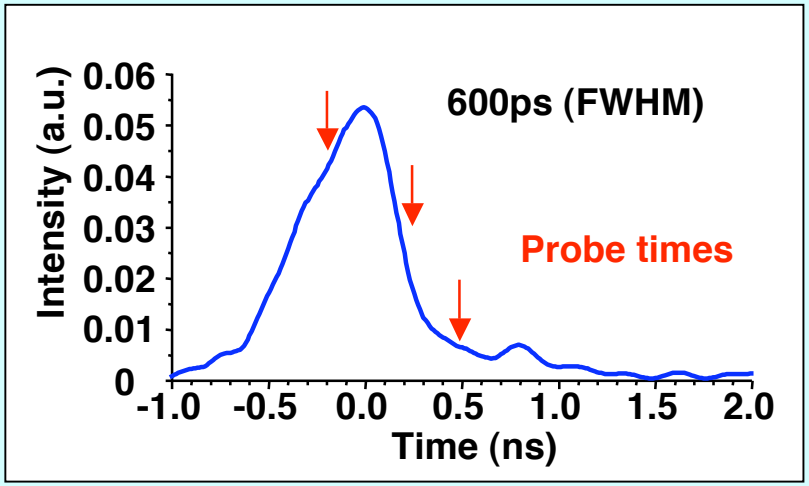

- Close agreement in density profile despite complicated plasma structure
- Probing within 10 μm of target surface yields accurate data

Understanding LPP through hydrodynamic simulation: Phenomena explained by energy transport mechanisms heating adjacent areas

Description

At early times ablation generated directly by laser heating. Laser energy deposited in square spatial profile to eliminate laser contribution from wings.

By peak of pulse, maximum temperature obtained in central narrow on-axis region from direct laser irradiation. Thermal x-rays heat region outside of laser spot generating cool plasma. Mass ablated slightly off-axis (black arrows) is initially normal to the target surface. Thermal pressure set up by the hot central region deflects and heats cooler mass sideways - sets up a double lobe structure and an on-axis density gradient.

(1) Half-moon or concave absorption front formed around the on-axis density dip reinforced by x-ray and electron thermal conduction from the hot corona. (2) Regions laterally removed from direct laser irradiation are heated by x-rays establishing a cool plasma progressively further from the laser focal region. This is then heated by thermal electron conduction resulting in enhanced ablation. The concave profile persists, the process continues and the lateral dimension of the plasma increases with mass ejected normal to target.

Figure

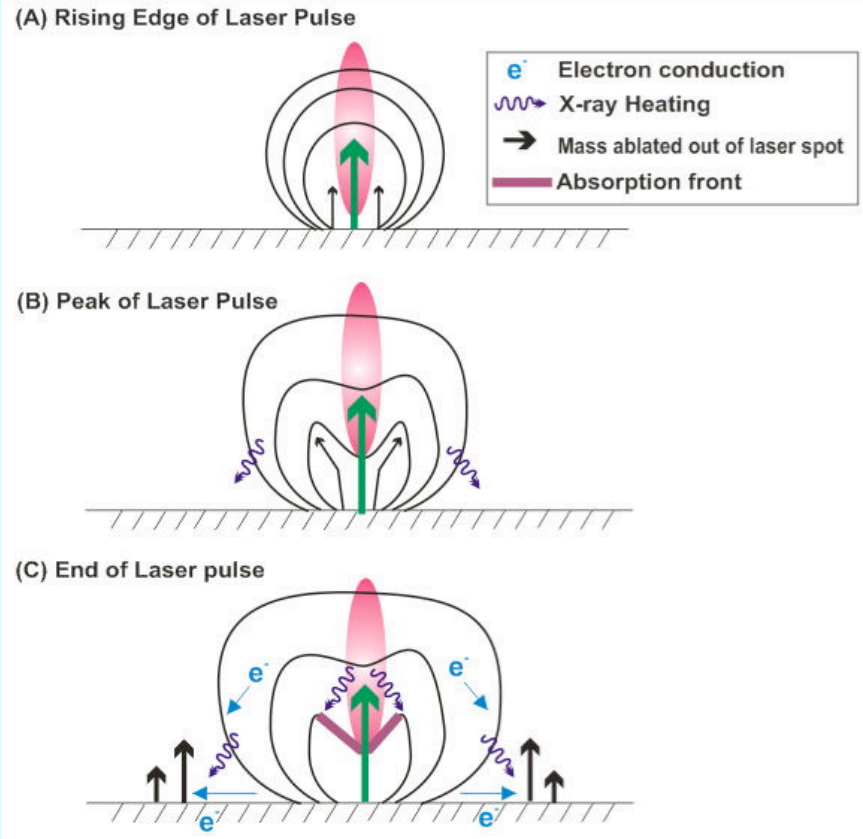

Following simulations are generated using square spatial profile and actual laser temporal pulse shape

Time slices show evolution of plasma during laser energy deposition, lateral heating generates new ablation outside of focus

Early time at -0.5 ns before laser peak

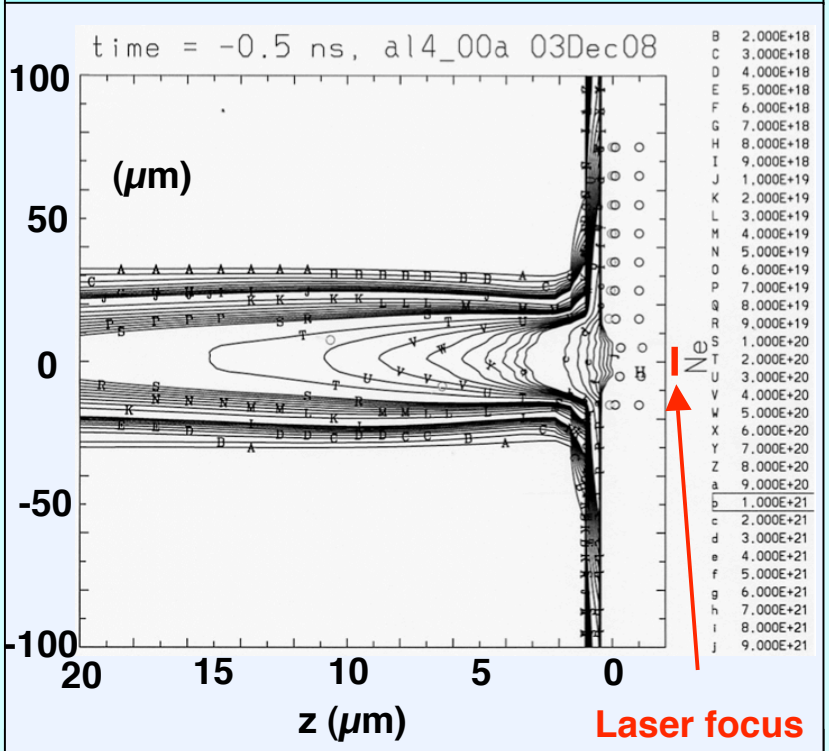

- Density profile is convex as expected during laser beam turn on
- Not much plasma formation outside of focal spot

300 ps later at -0.2 ns before laser peak

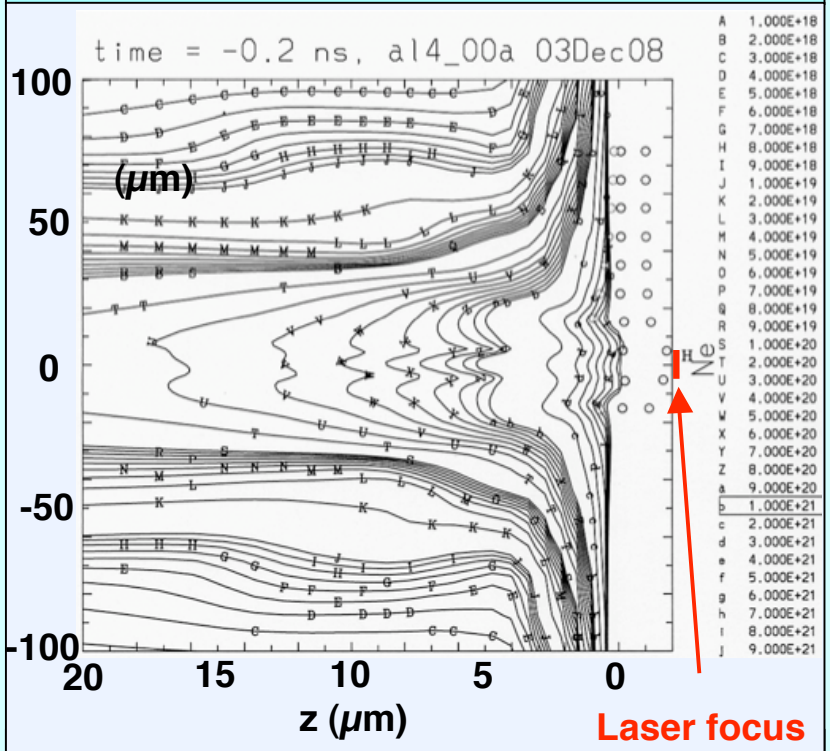

- Density profile begins to be structured on-axis
- Plasma formation outside of focal spot begins to increase rapidly

Plasma concave profile forms on rising edge of laser pulse, lateral heating continues to generate strong ablation outside of focus

At laser peak, t = 0 ns

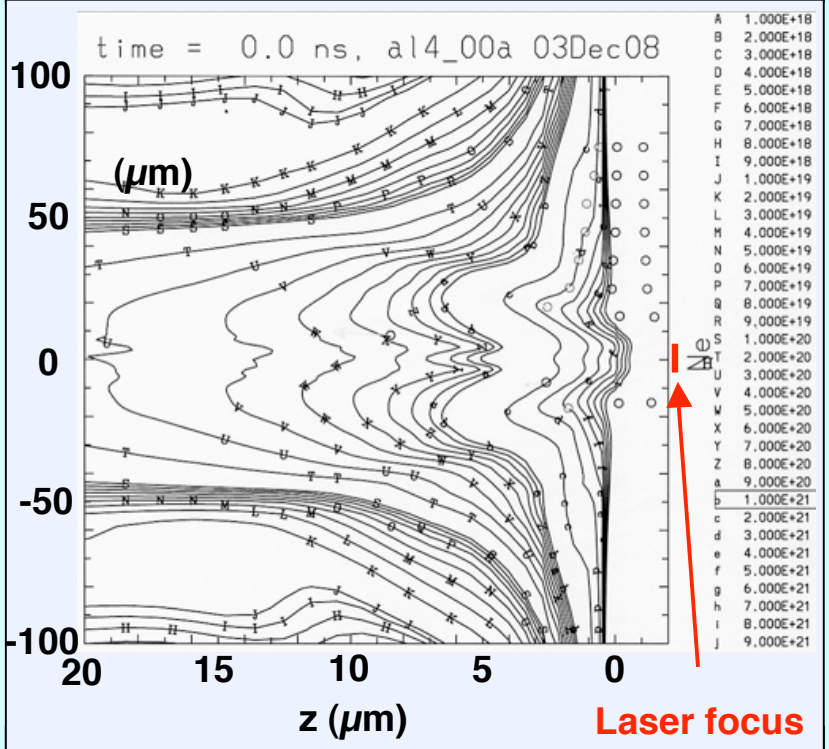

- Density profile is now concave above critical density
- More mass being ablated from outside of focal spot

t = +0.3 ns after laser peak

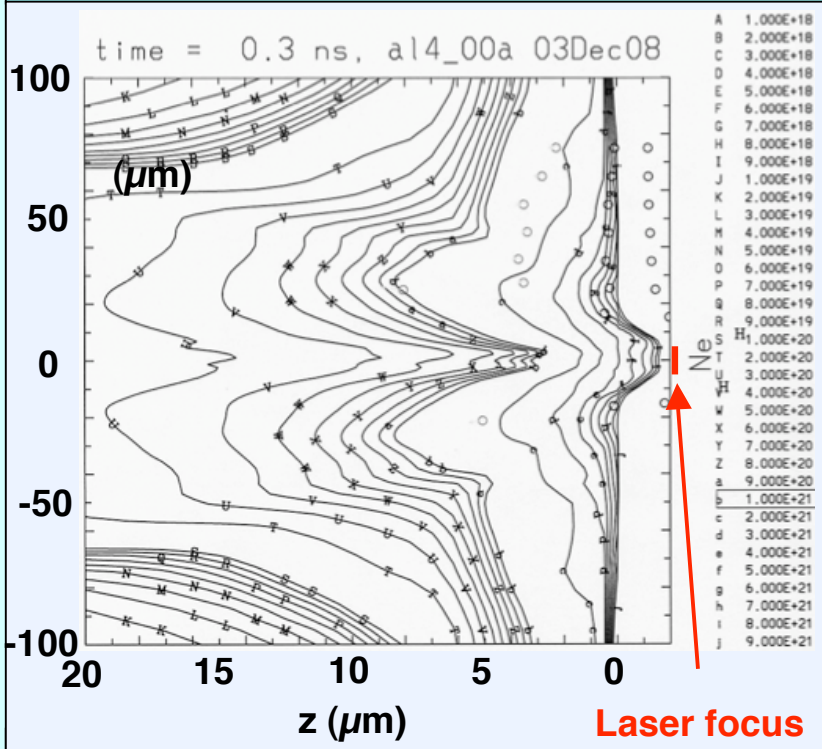

- Density profile is concave and extends to under-dense region establishing strong on-axis density dip
- Tracer particles show mass being ablated normal to target

Plasma concave profile persists to end of and beyond laser pulse

At end of laser pulse, t = +0.5 ns

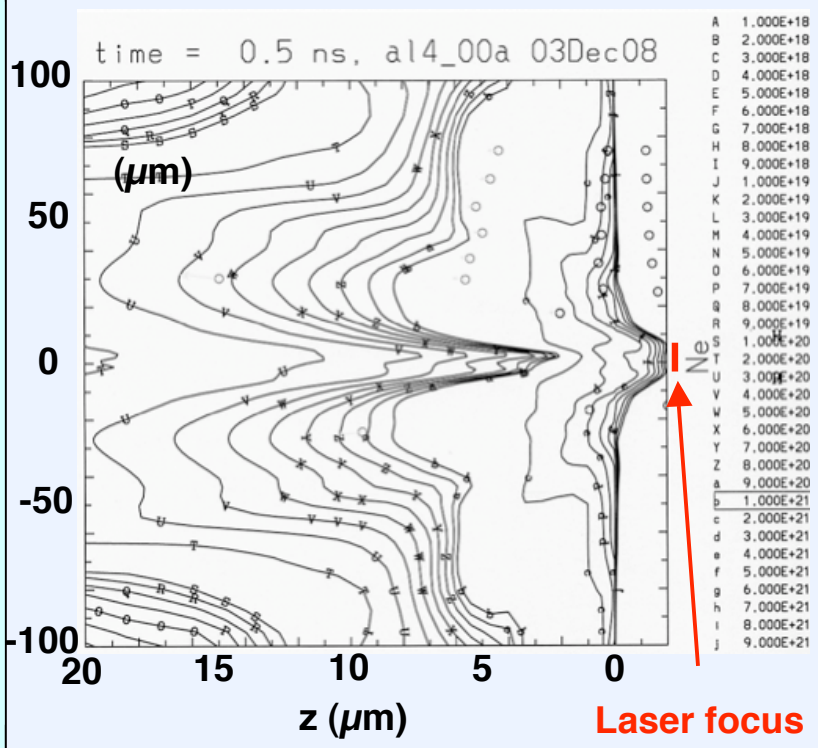

- Density profile is concave above critical density
- More mass being ablated from outside of focal spot

Observed phenomena with production of dense side lobes is observed in wide focal spot cases

Al target heated with 10 μm square spatial profile

Al target heated with 100 μm square spatial profile

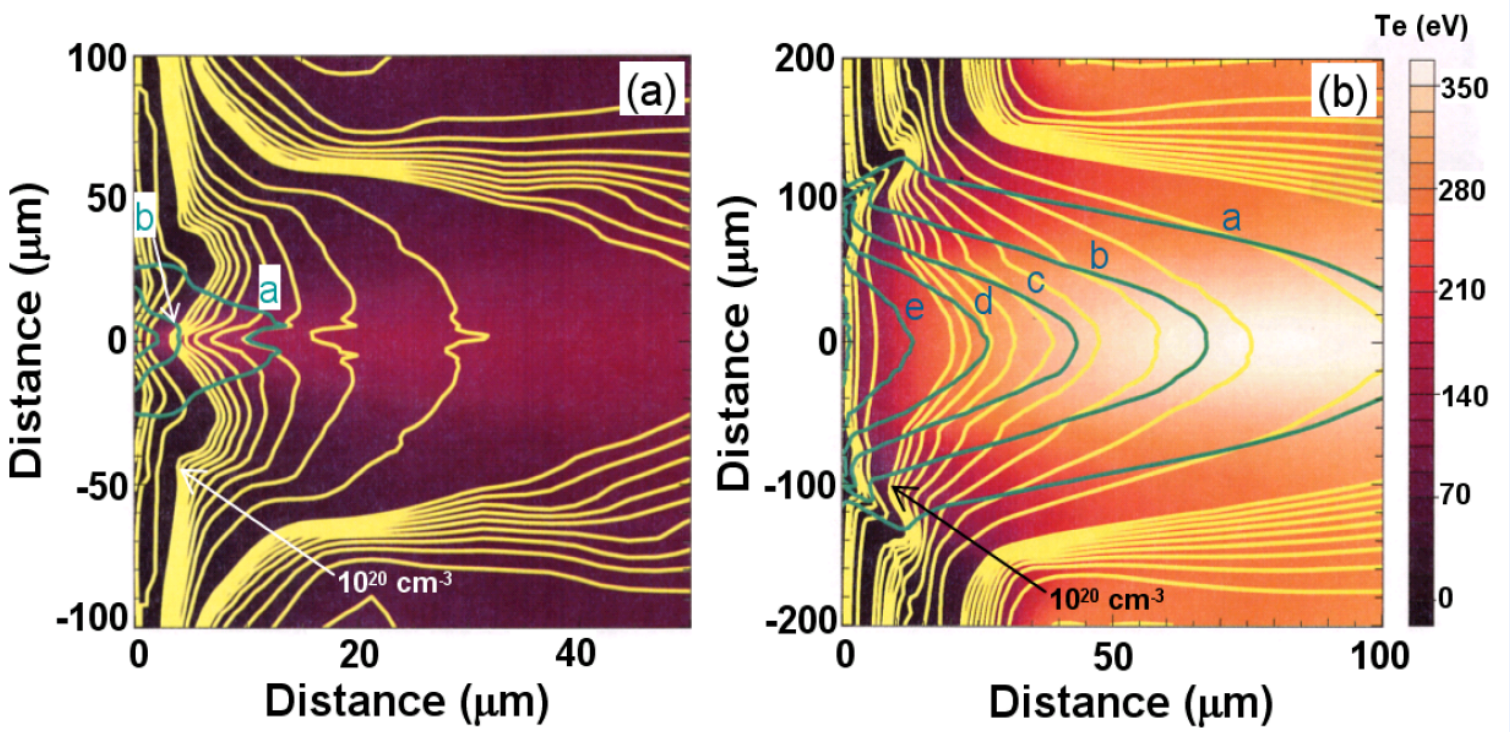

- T_e and plasma pressure are higher for 100 μm case due to radiative heating and 1D nature of plasma
- Simulations shown at t = 0 ns

Summary

(1) Tabletop x-ray laser interferometry is unique diagnostic for probing high energy density plasma phenomena

(2) Laser-produced plasma spatial profile can be observed very close to target surface due to short wavelength and picosecond pulse duration of probe

(3) Concave density profile and strong lateral heating produce plasma ablated outside of laser focus

(4) Non-local x-ray heating and strong thermal electron heat conduction are main mechanisms

(5) XRL interferometry can benchmark hydrocodes for various geometries 1-D, 2-D, converging, colliding plasmas, radiatively driven, surface release to give better understanding of physical processes

Appendix: How we determine density from ps interferograms of 5 mm Al line focus plasma

Experimental Setup and Laser Parameters

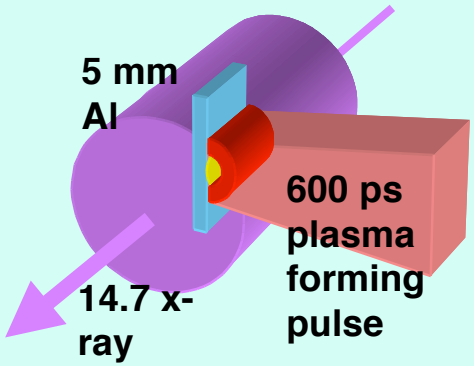

Δt = 0.7 ns

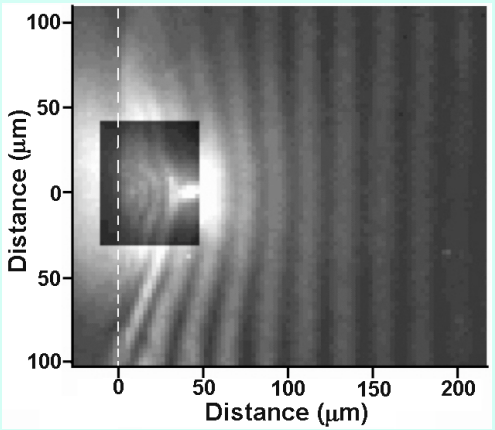

- I = 4 x 10^{11} W cm^{-2}, 600 ps (FWHM), 0.4 J at 1054 nm, 40 μm (FWHM) x 6 mm focus
- Delay line on 600 ps pulse allows XRL to probe plasma at Δt = 0, 0.5, 1 and 2 ns relative to the peak of pulse
- Absolute timing <100 ps, XRL pulse duration ≤ 10 ps

Density Measurements

(1) $n_{crit} = 1.1 \times 10^{21} \lambda^{-2}$ (cm^{-3}, λ in μm)

(2) $n_{ref} = \sqrt{1 - n_e / n_{crit}}$

(3) $N_{fringe} = \frac{\delta\phi}{2\pi} = \frac{1}{\lambda}\int_0^L (1 - n_{ref})dl \approx \frac{n_e}{2n_{crit}}\frac{L}{\lambda}$

(4) $N_{fringe} = 6.68 \times 10^{-20} n_e L$ (n_e in cm^{-3}, L in cm)

$\lambda = 147$ Å, $(1.47 \times 10^{-6}$ cm)

$n_{crit} = 5.09 \times 10^{24} cm^{-3}$

$L = 0.508$ cm

- 1 fringe shift gives n_e = 2.95 x 10^{19} cm^{-3}
- Minimum density increment (from fringe shift detection), Δn_e = 2.2 x 10^{18} cm^{-3}
- Observe 4 fringe shifts at Δt = 0.5 ns corresponding n_e = 1.2 x 10^{20} cm^{-3}

Appendix II: X-ray laser beam is stable, repeatable, has excellent coherence and fringe visibility with 4 - 6 ps duration

XRL Coherence and Fringe Visibility

(a)

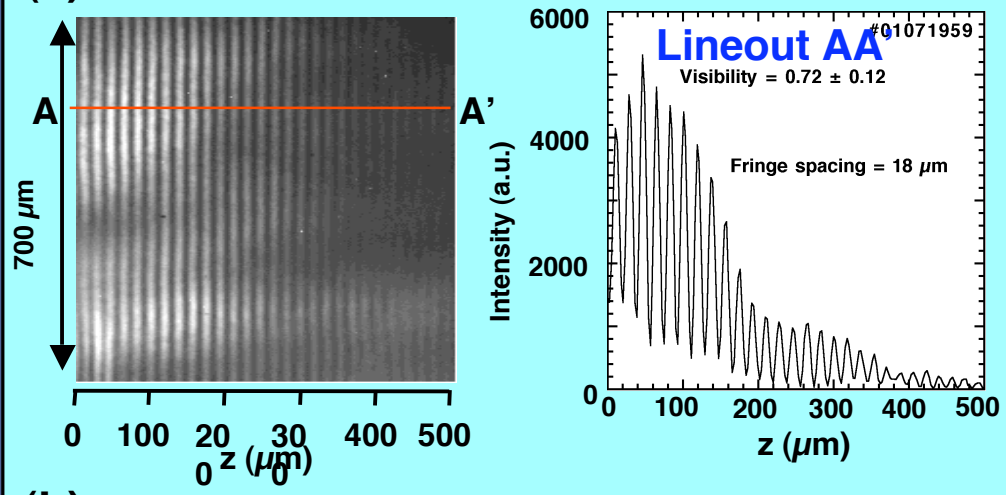

(b)

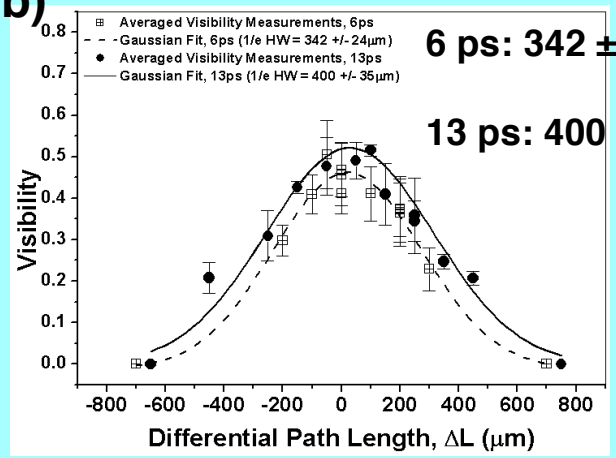

6 ps: 342 ± 24 μm 1/e HW

13 ps: 400 ± 35 μm 1/e HW

XRL Pulse vs SP duration

(c)

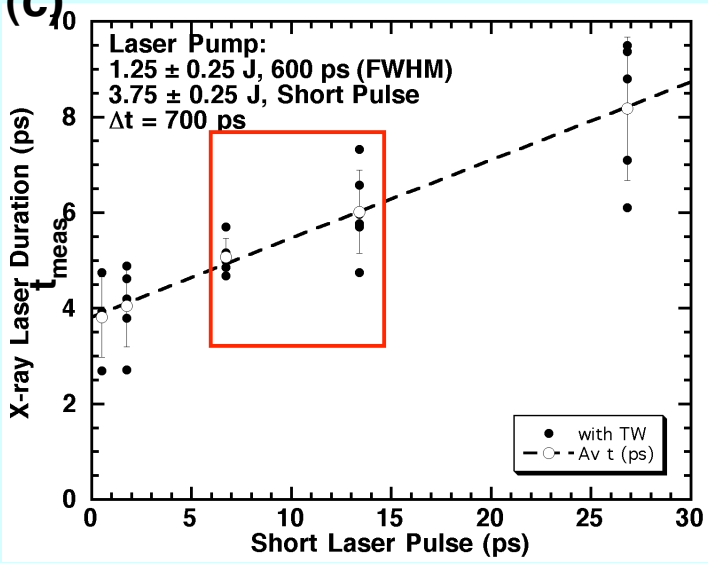

With R. Shepherd, R. Booth

(a) **Excellent spatial coherence - high fringe visibility 0.72 ± 0.12**

(b) **Excellent longitudinal coherence - Michelson interferometry (With P. Zeitoun, S. Hubert et al LIXAM/CEA)**

(c) **X-ray laser pulse duration 4 - 6 ps (FWHM) for interferometry**

Appendix III: X-ray Laser Mach-Zehnder Interferometers have been used to probe laser-generated plasma experiments

Interferometer with Multilayer Beamsplitters on NOVA

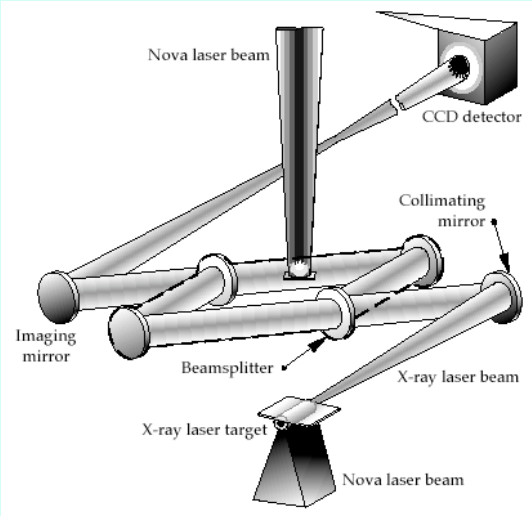

Da Silva *et al*, PRL 74, 3991 (1995).

- NOVA XRL, 155 Å, 5 mJ, 350 ps
- Thin film multi-layer beamsplitters used - delicate, technically challenging to fabricate
- Throughput of each arm ~0.018

Interferometer with Grazing Incidence Diffraction Grating Beamsplitters

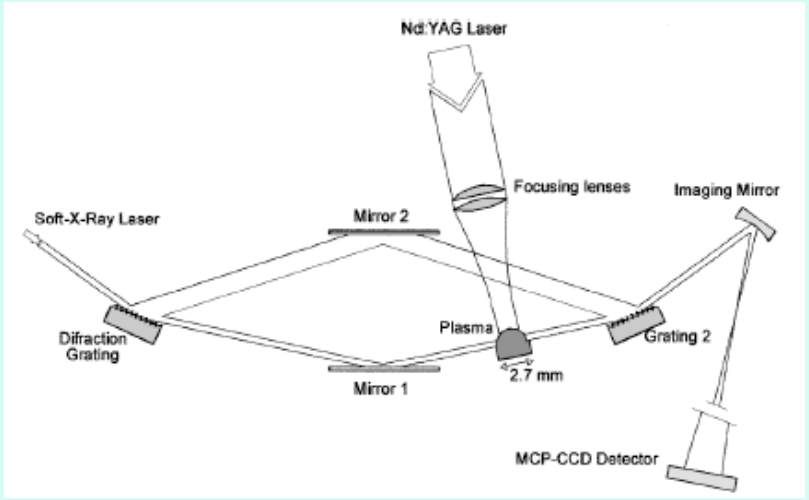

Filevich *et al*, Opt. Lett. 25, 356 (2000).

- Capillary discharge XRL, 46.9 nm, 0.13 mJ, 1 ns
- Grazing incidence grating beamsplitters used - robust, well-established grating technology
- Throughput of each arm ~0.057

High throughput of DGI well-suited to picosecond x-ray lasers

Appendix IV: Diffraction Grating 14.7 nm Ni-like Pd X-ray Laser Interferometer Layout for Mach-Zehnder configuration

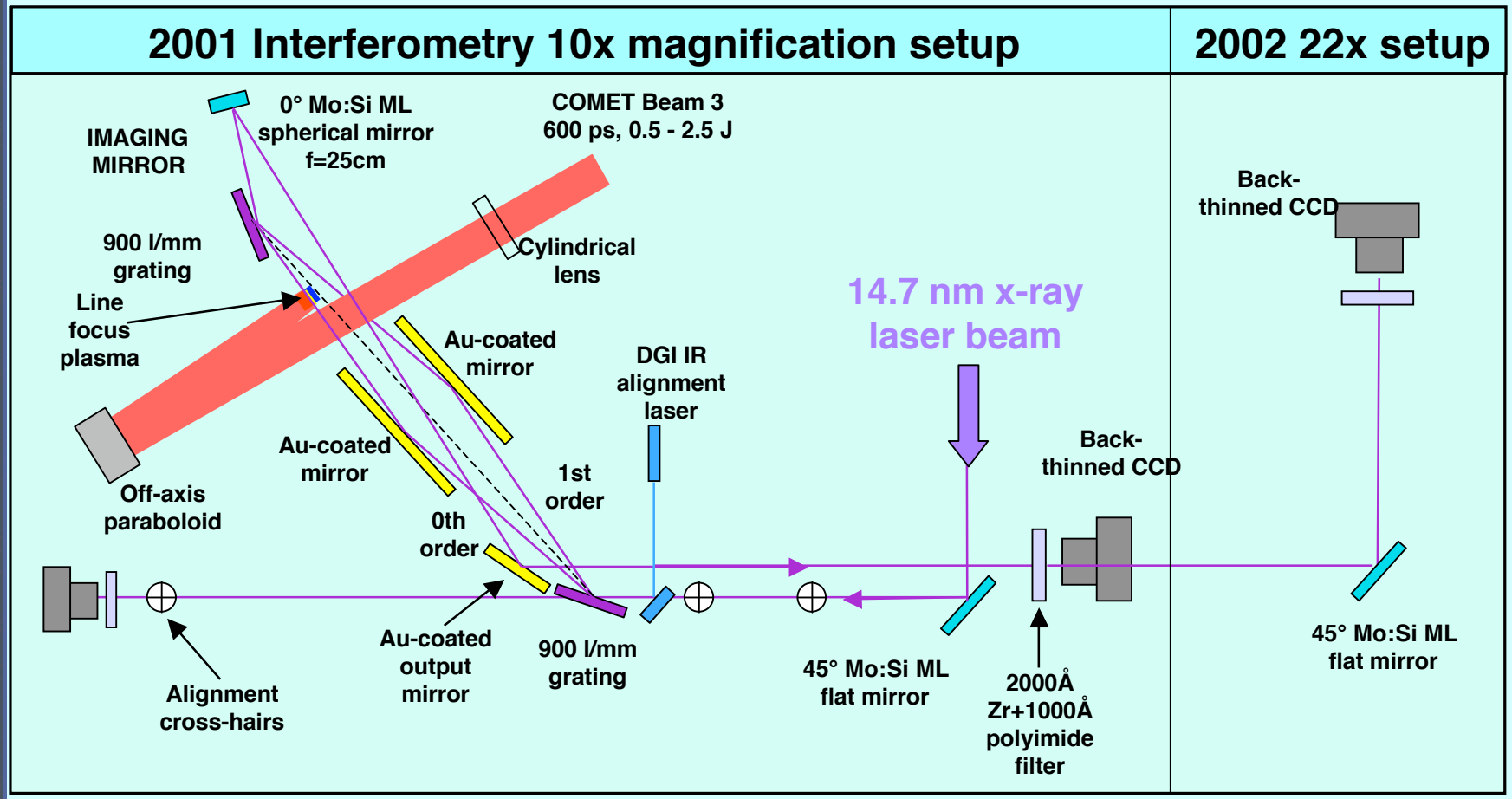

Detector spatial resolution of 0.5 μm achieved with 22x setup